Catal Lett (2008) 120:261–273
DOI 10.1007/s10562-007-9279-2

Investigation of 12-Tungstophosphoric Acid Supported on $Ce_{0.5}Zr_{0.5}O_2$ Solid Solution

G. Ranga Rao · T. Rajkumar

Received: 1 June 2007 / Accepted: 13 September 2007 / Published online: 2 October 2007

Abstract The nature of the Keggin ions of tungstophosphoric acid interacting with $Ce_{0.5}Zr_{0.5}O_2$ solid solution has been investigated. The vibrational study shows additional IR features at 1051 and 957 cm^{-1} which are correlated to the primary Keggin anions interacting with Lewis sites involving Ce^{4+} and Zr^{4+} ions, and thus affecting the P–O and W=$O_{terminal}$ bonds. The IR study indicates the formation of interfacial Ce^{4+}–O–W and Zr^{4+}–O–W bonds. The chemisorbed Keggin molecular layers on $Ce_{0.5}Zr_{0.5}O_2$ show activity towards conversion of acetophenone to styrene by Meerwein–Ponndorf–Verley reduction followed by dehydration. The activity is correlated with the relative intensities of IR peaks at 1051 and 957 cm^{-1} of the perturbed Keggin molecular layers.

Keywords $Ce_{0.5}Zr_{0.5}O_2$ solid solution · Tungstophosphoric acid · Keggin molecular layers · FTIR · Styrene

1 Introduction

In recent years, $Ce_xZr_{1-x}O_2$ solid solutions have been extensively investigated for variety of applications [1–6] and their catalytic properties are tested for number of vapour and liquid phase reactions [3–9]. It has been recognized that ceria is a crucial promoting component due to its strong redox as well as mild acid–base bifunctional properties. The $Ce_xZr_{1-x}O_2$ solid solutions are of particular importance due to the incorporation of Zr^{4+} ions in the cubic lattice of ceria and show surface $O^{2-} \rightarrow Ce^{3+}$ and $O^{2-} \rightarrow Ce^{4+}$ charge transfer transitions in UV region, and the combination and overtone bands of surface hydroxyl species in NIR region [2]. This is an evidence for the presence of surface O^{2-}–Ce^{3+}, O^{2-}–Ce^{4+} sites and –OH groups attached primarily to Zr^{4+} ions giving rise to both acid and base properties [10]. The surface structural changes and non-stoichiometry introduced by Zr^{4+} incorporation can lead to surface acid–base pair sites. These mild acid–base pairs formed by coordinatively unsaturated Zr^{4+}, Ce^{3+}, Ce^{4+} (Lewis acidic) and oxygen ions (Lewis basic) on $Ce_xZr_{1-x}O_2$ solid solutions assist various molecules including water to adsorb dissociatively or undissociatively. It is, therefore, interesting to use these materials as supports for studying the interaction and the stability of heteropoly acids (HPA). HPAs are heteropolyoxometalates consisting of metal-oxygen octahedra and PO_4 tetrahedron as basic structural units. The most useful HPAs in catalysis are the Keggin-type with general formula $[XM_{12}O_{40}]^{x-8}$ where X is the central heteroatom (Si^{4+}, P^{5+}, etc), x its oxidation state and M is the metal ion such as W^{6+}, Mo^{6+}. The negative charge on $XW_{12}O_{40}^{3-}$ unit can be compensated by hydrogen ions or by external cations with which the negative unit is interacting. The heteropoly acids are dispersed generally on acidic or neutral supports such as silica, silica gel [11, 12], carbon [13], mesoporous materials exemplified by MCM-41, zeolite Y [14–17] and layered clays [18]. The heteropoly acids are unstable in aqueous solutions at high pH and understandably the Keggin structure readily decomposes on basic solids such as MgO [19].

The nature of chemical interaction and bonding, dispersion, thermal stability and catalytic activity of HPAs depend to a large extent on the nature of solid support

G. Ranga Rao (✉) · T. Rajkumar
National Centre for Catalysis Research,
Department of Chemistry, Indian Institute of Technology
Madras, Chennai 600 036, India
e-mail: grrao@iitm.ac.in

carrier and HPA loading. Solid HPAs possess purely Brönsted acidity and the acid strength of crystalline HPAs decreases in the series PW > SiW > PMo > SiMo which is identical with the acid strengths shown in solutions [20]. It is, therefore, relatively simple to produce heteropoly anion in case of 12-tungstophosphoric acid (H_3PW) and these anions can strongly interact with Lewis acidic sites such as Zr^{4+} and Ce^{4+} present on $Ce_xZr_{1-x}O_2$ supports providing wide range of acid and redox properties in the solid state. The $Ce_xZr_{1-x}O_2$ solid solutions can be potential supports for heteropoly anion molecules because of their neutral or mild acid–base nature and good redox properties. To our knowledge, there has been one report where the removal of NO_x is studied on $H_3PW_{12}O_{40} \cdot 6\ H_2O$ supported on $Ce_xZr_{4-x}O_8$ [21]. We chose to investigate $Ce_{0.5}ZrO_{0.5}O_2$ solid solution which contains mild Lewis acid and base sites on the surface [2, 10] and is expected to show balanced acid–base properties due to statistically equal number of Zr^{4+} and Ce^{4+} ions present in the lattice. These surface sites along with oxygen ion vacancies associated with Ce^{3+}/Ce^{4+} redox centers can interact with heteropoly anion species. On SiO_2 surface H_3PW is known to produce two HPA species with characteristic ^{31}P MAS NMR signals at –15 ppm for intact Keggin structure and –14 ppm for species proposed as $(SiOH_2^+)(H_2PW_{12}O_{40}^-)$, more recently as $H_6P_2W_{18}O_{62}$ or $H_6P_2W_{21}O_{71}$ [22, 23]. There are number of experimental studies on silica and zeolite supported 12-tungstophosphoric acid which include XRD [11–13, 15, 16, 20], IR [11–14, 19], Raman [22, 24], ^{31}P magic–angle spinning NMR [11, 14–16, 18, 23] and recently polyoxoanion surface chemistry by invoking Stranksi–Krastanov growth adsorption mode of forming monolayer using surface elemental analysis method [22].

In this study, the $Ce_{0.5}Zr_{0.5}O_2$ solid solution was synthesized by a new route combining both sol–gel and combustion methods to obtain high quality ceramic powders for supporting heteropolyanions. The citric acid sol–gel combustion method is one type of non-alkoxide sol–gel method, which is an efficient method for the preparation of nanocrystalline inorganic oxides [25, 26]. In the present work, the stability and structural changes taking place in heteropoly anion species interacting with $Ce_{0.5}ZrO_{0.5}O_2$ solid solution have been investigated by XRD, IR, Raman, TPR, NH_3-TPD, ^{31}P MAS NMR, sorption, UV–Vis–DRS, TEM and SEM methods. The nature of bonding between Ce^{4+} sites and $PW_{12}O_{40}^{n-}$ Keggin units and their stabilization is discussed. The Meerwein–Ponndorf–Verley (MPV) type reduction followed by dehydration has been carried out as a test reaction on $H_3PW/Ce_{0.5}ZrO_{0.5}O_2$ catalysts. The vapour phase synthesis of styrene from acetophenone and propan-2-ol is presented in Scheme 1.

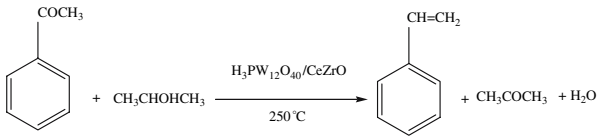

Scheme 1 Conversion of acetophenone to styrene

2 Experimental

2.1 Preparation of $H_3PW/Ce_{0.5}Zr_{0.5}O_2$ Catalysts

The $Ce_{0.5}Zr_{0.5}O_2$ powders were prepared by using sol–gel combustion method [2, 26]. The starting materials of cerium nitrate, zirconyl nitrate, citric acid and ammonia of analytical purity were used as received from CDH (India). Stoichiometric amounts of $Ce(NO_3)_3 \cdot 6H_2O$ and $ZrO(NO_3)_2 \cdot xH_2O$ were dissolved in 100 mL deionized water and equimolar citric acid to Ce + Zr was then added to the aqueous solution. The mixed solution was maintained at pH > 7 by adding aqueous ammonia. The gel formed was evaporated to dryness at 100 °C in an oven. The dried sample was introduced into a furnace at 350 °C in air. The sample had combusted itself completely in a self-propagating manner producing fine powders. The powders were then calcined at 500°C for 2 h in air. However, sol–gel combustion method does not seem suitable for preparing pure zirconia phases. Zirconia was prepared by fast combustion method [2]. In this method $ZrO(NO_3)_2 \cdot xH_2O$ was dissolved in minimum quantity of water and ignited at 350 °C in a furnace by using carbohydrazide (CH_2N_4O) as fuel. The $H_3PW/Ce_{0.5}Zr_{0.5}O_2$ catalysts were prepared by wet impregnation of aqueous H_3PW on $Ce_{0.5}Zr_{0.5}O_2$ support. The H_3PW aqueous solution was added drop wise to the support dispersed in water by continuous stirring at room temperature. The samples were dried at 100 °C overnight and calcined at 250 °C for 2 h in air.

2.2 Characterization

The specific surface areas of samples were determined by BET method using N_2 adsorption/desorption at –196 °C on Micromeritics ASAP 2020 surface area analyzer. All samples were out-gassed at 100 °C for 2 h followed by 300 °C for 10 h in dynamic vacuum before physisorption measurements. Pore size distributions were determined from the measured desorption isotherms using BJH method. The surface area and pore volume (single point adsoprtion at $p/p_0 = 0.99$) decrease consistently with H_3PW loading (Table 1). All samples were analysed by X-ray diffraction employing Shimadzu XD-D1 diffractometer using Cu K_α radiation (λ = 1.5418 Å).

Table 1 Physicochemical characteristics of $H_3PW/Ce_{0.5}Zr_{0.5}O_2$ catalysts

Sample	BET surface area (m^2 g^{-1})	Total pore volume (cm^3 g^{-1})
CeO_2	41	0.124
$Ce_{0.5}Zr_{0.5}O_2$	43	0.086
10 wt.% $H_3PW/Ce_{0.5}Zr_{0.5}O_2$	32	0.067
20 wt.% $H_3PW/Ce_{0.5}Zr_{0.5}O_2$	32	0.046
30 wt.% $H_3PW/Ce_{0.5}Zr_{0.5}O_2$	22	0.028
40 wt.% $H_3PW/Ce_{0.5}Zr_{0.5}O_2$	23	0.035
50 wt.% $H_3PW/Ce_{0.5}Zr_{0.5}O_2$	21	0.022

The IR spectra of different samples (as KBr pellets) were recorded using Perkin–Elmer infrared spectrometer with a resolution of 4 cm^{-1}, in the range of 400–4000 cm^{-1}. The Raman spectra were recorded using Bruker FRA-106 FT-Raman spectrometer with beam power of 20 mW and resolution of 4 cm^{-1} in the range of 50–3500 cm^{-1}.

The UV–Vis spectroscopic studies were carried out in diffuse reflectance mode. UV–Vis–NIR spectra were recorded on Varian Cary 5E spectrometer equipped with an integrating sphere coated with polytetrafluoroethylene (PTFE) in the spectral range of 200–2500 nm. The spectra are presented as F(R), Kubelka–Munk function versus incident photon wavelength.

The ^{31}P MAS NMR spectra of $H_3PW/Ce_{0.5}Zr_{0.5}O_2$ were recorded using Bruker Avance 400 spectrometer at resonance frequency of 161.97 MHz for ^{31}P nuclei with Bruker CP MAS probe and the chemical shifts are reported in ppm (δ) relative to external 85 wt.% H_3PO_4. The ^{31}P MAS NMR spectra were recorded with a sample spinning rate of 8 kHz, and the delay between two pulses was 2 s for relaxation of the ^{31}P nuclei.

Scanning electron microscopy (SEM) pictures were taken using FEI Quanta 200 microscope. The sample powders were deposited on a carbon tape before mounting on a sample holder. The TEM images of the samples were taken using JEOL JEM-3010 transmission electron microscope. The material was dispersed in acetone and deposited onto a 200-mesh size carbon-coated copper grid. The TEM images were recorded with a slow-scan CCD camera.

The redox behaviour was examined by temperature-programmed reduction (TPR) on Micromeritics Chemisorb 2750 instrument. All the samples were pretreated in Ar flow of 20 mL per min at 200°C for 30 min. The reducing gas used in all TPR experiments was 5% H_2 in Ar with a flow rate of 20 mL min^{-1}. The temperature range explored was from room temperature to 800 °C with a linear heating rate of 10 °C min^{-1}. The water produced by reduction was trapped in slurry of isopropyl alcohol cooled by liquid nitrogen.

All the $H_3PW/Ce_{0.5}Zr_{0.5}O_2$ samples including H_3PW and $Ce_{0.5}Zr_{0.5}O_2$ were analysed by temperature-programmed desorption (TPD) of NH_3 using Chemisorb 2750 instrument. The TPD experiments were carried out on pre-calcined samples at 250 °C for 2 h. Typically 20 mg of sample was loaded and pre-treated at 200 °C in He for 1 h. The temperature was decreased to 100 °C under a flow of helium, and then saturated with 9.34% NH_3 in He gas mixture for 1 h, followed by flushing with pure He gas to remove physisorbed ammonia for 15 min at 100 °C. Then the sample was cooled to room temperature in He flow. NH_3 was desorbed in He flow by increasing the temperature from room temperature to 800 °C at the rate of 10 °C min^{-1}, and NH_3 desorption was measured with TCD detector.

2.3 Catalytic Experiments

Vapour phase hydrogenation–dehydration of acetophenone by using propan-2-ol as the hydrogen donor was carried out in a fixed-bed flow glass reactor (i.d.: 2.2 cm, length: 30 cm) kept in a hot zone of a cylindrical furnace mounted vertically. About 0.5 g of catalyst was loaded in the middle of the reactor and supported on either side with a thin layer glass wool and glass beads in order to maintain constant flow of the reactants into the catalyst bed. The temperature was monitored by thermocouple, which is kept at the middle of the catalyst bed. Prior to the reaction, the catalyst was preheated in pure oxygen flow (20 mL min^{-1}) for 2 h at 300 °C and the catalytic tests were performed at 250 °C under atmospheric pressure using nitrogen carrier gas flow 30 mL min^{-1}. The reactants were injected into the reactor at a rate of 4 mL h^{-1} using a syringe infusion pump (SP-01 model, Miclins India). The liquid products were collected in an ice trap and analyzed by a gas chromatograph (AMIL-Nucon 5765) using a HP-1 capillary column (cross-linked methyl silicone gum, 25 m × 0.2 mm × 0.33 μm film thickness) and a flame ionization detector. The FID response factors were established by multi-point calibration using pure reagents and their mixtures for quantification.

3 Results and Discussion

3.1 X-ray Diffraction Study

The citrate sol–gel combustion synthesized CeO_2 and $Ce_{0.5}Zr_{0.5}O_2$ solid solution samples are used in this study. Figure 1 shows the powder X-ray diffraction (PXRD) pattern of cubic CeO_2, $Ce_{0.5}Zr_{0.5}O_2$, H_3PW and $Ce_{0.5}Zr_{0.5}O_2$ supported H_3PW samples. There is a clear shift in

2θ value of (111) reflection and others confirming the formation of cubic $Ce_{0.5}Zr_{0.}5O_2$ solid solution due to the substitution of smaller Zr^{4+} ion (ionic radius 0.084 nm) in place of Ce^{4+} ion (ionic radius 0.097 nm). The lattice parameter decreases from 0.542 nm for CeO_2 to 0.516 nm for $Ce_{0.5}Zr_{0.5}O_2$. According to recent studies, citrate complexing method yields stable textural properties for $Ce_{0.5}Zr_{0.5}O_2$ composition [27] and it can exhibit variety of phases differing in cation ordering [28]. The PXRD of H_3PW in Fig. 1(a) shows complex pattern with intense reflection at $2\theta = 8.5$. It is known that the structure of H_3PW changes with heat treatment [15, 16] and due to the loss of water molecules [29]. However, the present study does not show any significant reflections attributable to supported 10–50 wt.% H_3PW, other than those related to the cubic $Ce_{0.5}Zr_{0.5}O_2$ support (Fig. 1d–h). The PXRD profiles of H_3PW on $Ce_{0.5}Zr_{0.5}O_2$ are entirely different from H_3PW supported on silica and MCM-41 where the reflections due to dispersed H_3PW are absent only up to 20 wt.% [11–13, 23]. Interestingly, $H_3PW \cdot 26H_2O$ supported on the dealuminated zeolite Y matrix also do not show XRD lines at low loadings until about 15 wt.%, beyond which the cubic phase of $H_3PW \cdot 26H_2O$ is stabilized [15, 16]. However, in this study, the formation of such a cubic phase is elusive on $Ce_{0.5}Zr_{0.5}O_2$ solid solution.

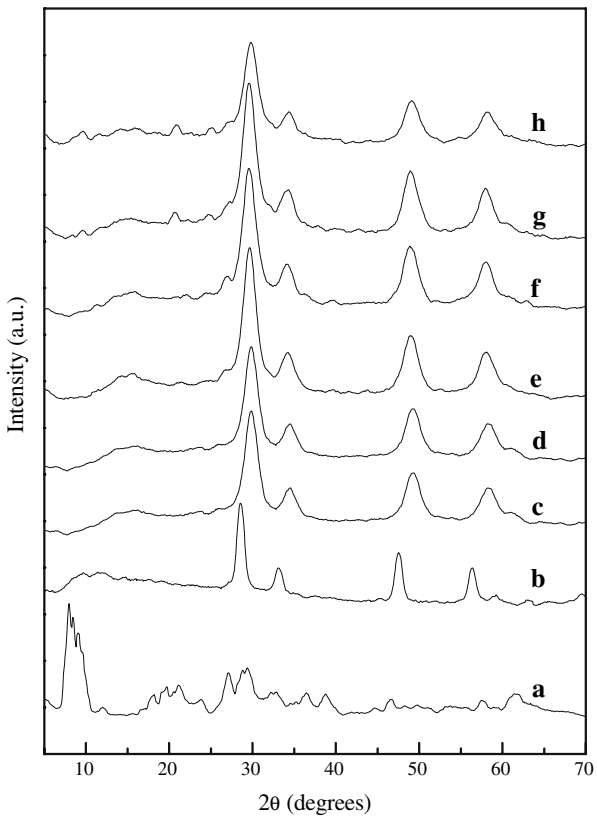

Fig. 1 XRD pattern of (**a**) H_3PW, (**b**) CeO_2, (**c**) $Ce_{0.5}Zr_{0.5}O_2$, (**d–h**) 10, 20, 30, 40, 50 wt.% of H_3PW dispersed on $Ce_{0.5}Zr_{0.5}O_2$

This essentially shows that the dispersion behaviour of Keggin ions appears unique on $Ce_{0.5}Zr_{0.5}O_2$ solid solution and the H_3PW crystallinity is severely disrupted for 10–50 wt.% H_3PW loadings. This is a first indication that the physical and chemical nature of the dispersed Keggin anion units, $PW_{12}O_{40}^{3-}$, on $Ce_{0.5}Zr_{0.5}O_2$ is different from that of SiO_2, MCM-41 or zeolite supports. In the present case, the surface area of $Ce_{0.5}Zr_{0.5}O_2$ is 43 m^2/g and by taking the size of the $PW_{12}O_{40}^{3-}$ molecular unit as $\sim$1 nm, it requires approximately 8.3×10^{-5} moles of Keggin molecular units per gram of $Ce_{0.5}Zr_{0.5}O_2$ support to obtain a molecular layer of $PW_{12}O_{40}^{3-}$ units ($\sim$24% H_3PW loading). According to this assumption we would have about two molecular layer thickness of $PW_{12}O_{40}^{3-}$ units for 50 wt.% H_3PW dispersed on the $Ce_{0.5}Zr_{0.5}O_2$ support. It appears that the Keggin units are not sufficiently aggregated and do not show crystalline nature in PXRD pattern in Fig. 1. The absence of H_3PW related reflections even above 20 wt.% loading on the $Ce_{0.5}Zr_{0.5}O_2$ support shows that the Keggin units are molecularly dispersed. This is confirmed by HRTEM study discussed in Sect. 3.8.

3.2 IR Study

In order to understand the nature of Keggin units interacting with the $Ce_{0.5}Zr_{0.5}O_2$, we present in Fig. 2 the FT-IR spectra of dispersed 10–50 wt.% H_3PW species and $Ce_{0.5}Zr_{0.5}O_2$ support as well as the physical mixture of both. The heteropoly compounds are known to have primary, secondary and tertiary structures [18]. The molecular nature of solid heteropolyacid comes from its primary structure, which is essentially the structure of metal oxide cluster molecule (heteropolyanion). The $PW_{12}O_{40}^{n-}$ Keggin structure consists of central PO_4 tetrahedron which is surrounded by four threefold W_3O_{13} units formed by each WO_6 octahedron sharing two edges with other WO_6's. The four W_3O_{13} units are linked to one another by corner sharing O_{corner} atoms. The total assembly has a tetrahedral pocket in its center for P heteroatom. The $PW_{12}O_{40}^{3-}$ structure shows characteristic P–O stretching ($\sim$1083 cm^{-1}), $W–O_{terminal}$ stretching ($\sim$987 cm^{-1}), stretching of $W–O_c–W$ inter bridges between corner-sharing WO_6 octahedra ($\sim$891 cm^{-1}), stretching of $W–O_e–W$ intra bridges between edge-sharing WO_6 octahedra ($\sim$815 cm^{-1}) and P–O bending (596 cm^{-1}). The IR spectra of $PW_{12}O_{40}^{3-}$ ions on $Ce_{0.5}Zr_{0.5}O_2$ show the characteristic features in the range of 700–1200 cm^{-1} indicating that the primary Keggin structure is intact on oxide surface. The intrinsic IR absorption bands of $PW_{12}O_{40}^{3-}$ Keggin anion clearly appear at 1080 cm^{-1} (P–O), 982 cm^{-1} ($W=O_{terminal}$), 892 cm^{-1} ($W–O_{corner}–W$) and 812 cm^{-1} ($W–O_{edge}–W$) [14, 30]. In addition to these asymmetric stretching frequencies,

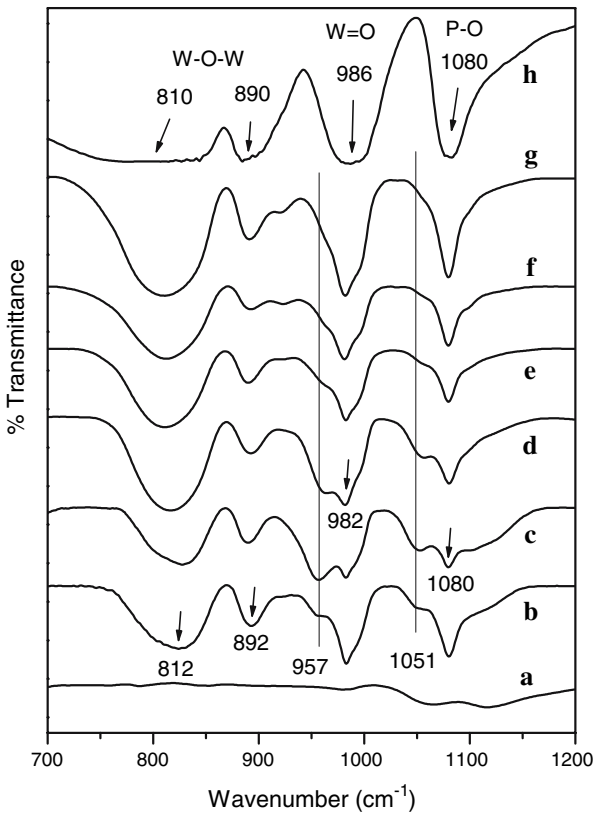

Fig. 2 FTIR spectra of (**a**) $Ce_{0.5}Zr_{0.5}O_2$, (**b**) physical mixture of 10 wt.% H_3PW + $Ce_{0.5}Zr_{0.5}O_2$, (**c**–**g**) 10, 20, 30, 40, 50 wt.% of H_3PW dispersed on $Ce_{0.5}Zr_{0.5}O_2$ support and (**h**) pure H_3PW

intense broad IR bands (not shown) have been observed at 3400 and 1635 cm^{-1} due to water of hydration. The degree of hydration of H_3PW samples supported on $Ce_{0.5}Zr_{0.5}O_2$ is quantified as hexahydrate based on the detailed study reported by Misono [18]. The $Ce_{0.5}Zr_{0.5}O_2$ solid solution powder does not show any of these bands in Fig 2(a). This suggests that the Keggin units are intact on $Ce_{0.5}Zr_{0.5}O_2$ and possibly structural changes have occurred. Unlike MgO, $Ce_{0.5}Zr_{0.5}O_2$ is mildly basic to decompose Keggin units readily. Interestingly, there are a couple of stronger non-intrinsic IR bands observed at 1051 and 957 cm^{-1} in Fig. 2, the intensity of both decreases as H_3PW loading increases from 10 to 50 wt.% on $Ce_{0.5}Zr_{0.5}O_2$ support. The new IR shoulder bands observed in this study at 1051 and 957 cm^{-1} are attributed, respectively, to P–O bonds and terminal W=O bonds of Keggin species directly interacting with Ce^{4+} and Zr^{4+} ions. The $PW_{12}O_{40}^{3-}$ molecular units can interact with Lewis sites through terminal oxygens of W=O bond leading to bond polarization which increases the bond length of W=O and thus affecting the P–O bond as well. The IR spectrum of the physical mixture also shows remnant shoulder peaks at 1051 and 957 cm^{-1} (Fig. 2b). This indicates that some Keggin ions are strongly interacting with Ce^{4+}/Zr^{4+} ions in the physical mixture as well. The M–O bond stretching vibrations in the $PW_{12}O_{40}^{n-}$ Keggin structure are predicted to be sensitive to the counter cation size and possibly to its polarizing power [30]. This scenario is expected to decrease the vibrational frequencies of P–O bonds and terminal W=O bonds which are red-shifted (bands at 1051 and 957 cm^{-1}) in the IR spectra (Fig. 2). In the bulk solid H_3PW, the W=O terminal oxygens are more accessible to water molecules to link four neighbouring heteropoly anions by forming hydrogen bonds. However, on $Ce_{0.5}Zr_{0.5}O_2$ solid solution the $PW_{12}O_{40}^{n-}$ Keggin anions resulting from H_3PW in aqueous solution can form $(M^{4+})[H_2PW_{12}O_{40}^{-}]$, $(M^{4+})[HPW_{12}O_{40}^{2-}]$ and $(M^{4+})[PW_{12}O_{40}^{3-}]$ surface species on the metal ion Lewis centers. The ionic type of interaction is expected to be more favourable in the case of reducible Ce^{4+} ions than Zr^{4+} ions, due to the redox nature of ceria, $Ce^{4+} \rightleftarrows Ce^{3+}$. This process can in principle generate variety of $(Ce^{4+})[H_2PW_{12}O_{40}^{-}]$, $(Ce^{4+})[HPW_{12}O_{40}^{2-}]$ and $(Ce^{4+})[PW_{12}O_{40}^{3-}]$ surface species involving $H_nPW_{12}O_{40}^{n-3}$ (n = 1, 2, 3) Keggin anions. However, the formation of $(Zr^{4+})[H_nPW_{12}O_{40}^{n-3}]$ species cannot be entirely ruled out. The development of new IR features at 1051 and 957 cm^{-1} suggests additional distortions and lowering of symmetry of PO_4 tetrahedra (T_d) and WO_6 octahedra (O_h) as a result of Keggin ion interaction with Ce^{4+} and Zr^{4+} ions. It is therefore inferred that there are at least two types of Keggin units on the oxide surface, one of which is directly interacting with surface cationic sites showing decreased IR stretching frequencies at 1051 and 957 cm^{-1}. These non-intrinsic IR bands, due to the interaction of terminal oxygens ($W{=}O_{terminal}$) of Keggin anion with Ce^{4+} ions and Zr^{4+} ions on $Ce_{0.5}Zr_{0.5}O_2$ oxide support, gradually disappear at higher H_3PW loadings leaving the characteristic bulk H_3PW IR bands at 1080, 982 and 892 cm^{-1} and 812 cm^{-1} intact. This shows that at higher loadings the Keggin units reach the limit of bulk like $H_3PW \cdot 6H_2O$, possibly disorderly packed structure. Thus at higher loadings the local interactions of Keggin ions with Lewis acid sites are masked by cohesive or hydrogen bonded interactions among the Keggin units on the $Ce_{0.5}Zr_{0.5}O_2$ support.

3.3 FT-Raman Study

We have used FT-Raman spectroscopy to obtain vibrational information of both on $Ce_{0.5}Zr_{0.5}O_2$ and the interacting $PW_{12}O_{40}^{n-}$ species. The symmetry of the optical absorption modes of fluorite structure is given by $\Gamma_{optical} = F_{1u}(IR) + F_{2g}$ (Raman). Therefore, FT-Raman spectroscopy is an exclusive method to identify the symmetric O–Ce–O vibrational stretching of the F_{2g} mode in the cubic fluorite ceria lattice at 465–467 cm^{-1} [31, 32]. In addition, it is also useful to detect the symmetric and asymmetric

stretching modes, respectively, of W=$O_{terminal}$ around 1007–1012 cm^{-1} and 990–998 cm^{-1}, as well as 217 cm^{-1} due to symmetric W–$O_{central}$ in Keggin ions [11, 30]. The FT-Raman spectra of CeO_2, $Ce_{0.5}Zr_{0.5}O_2$ and dispersed 10–50 wt.% H_3PW species on $Ce_{0.5}Zr_{0.5}O_2$ support are displayed in Fig. 3. The Raman spectrum (Fig. 3a) shows an intense Raman band at 468 cm^{-1} characteristic of O–Ce–O stretching of bulk CeO_2 sample. Upon substitution of 0.5 mol of Zr^{4+} ions in CeO_2, the Raman band has broadened asymmetrically towards lower frequencies up to 600 cm^{-1}, reduced in intensity and the peak blue shifted to 480 cm^{-1} which is in agreement with previous studies [1, 33, 34]. A single Ce–O bond length in pure CeO_2 is 0.236 nm. A recent EXAFS study shows that the Ce–O bond length varies with Zr substitution, which can be divided into a short category below 0.236 nm and a long category above 0.236 nm [33]. This may explain to a certain extent the broadening and the blue shift of Raman active O–Ce–O stretch observed in Fig. 3. The characteristic stretching modes in the W=O region of Keggin ions on $Ce_{0.5}Zr_{0.5}O_2$ are also observed in Raman at 1015, 997 and 232 cm^{-1}. These values are about 5 cm^{-1} higher than the W=O stretching frequencies reported on silica [11, 22]. The small blue shift in vibrational frequencies of Keggin unit has been predicted when protons are replaced by metal ions such as Na [30]. Such small blue shifts in W=O bonds are attributed to increased bond order and reported to occur due to the strength of interaction or structural changes of WO_x species at calcination temperatures greater than 500 °C [35–37]. In the present study, $PW_{12}O_{40}^{n-}$ ions seem to interact with reducible Ce^{4+} as well as Zr^{4+} sites and provide the basis for Raman bands seen in Fig. 3. Thus the Raman bands observed are likely to be attributed to $Ce^{4+}\cdots O^{\delta-}_{terminal}$=W as well as $Ce^{4+}\cdots O^{\delta-}_{terminal}$=W bonds formed between the surface metal ion sites and $H_nPW_{12}O_{40}^{n-3}$ (n = 0, 1, 2, 3). When the Keggin ion interacts with Ce^{4+} ion or Zr^{4+} ion through the oxygen end of the terminal W=O bond, one would expect weakening of W=O bond leading to changes in the symmetry of W tetrahedra and the shape of vibrational spectra, as observed in IR spectra in Fig. 2. However, unlike in IR spectra, subtle changes seem to have occurred in the Raman frequencies of Keggin species spread on $Ce_{0.5}Zr_{0.5}O_2$ surface. It has been reported that pure H_3PW Raman bands at 1012 and 990 cm^{-1} are red-shifted to 997 and 981 cm^{-1} when H_3PW is dispersed on pure ZrO_2 support suggesting the formation of W–O–Zr bonds (840 cm^{-1}) [36, 38]. However, in the present Raman study, there is an elusive evidence of formation of such bonded species on $Ce_{0.5}Zr_{0.5}O_2$ solid solution. The Raman bands at 1015, 997 and 232 cm^{-1} due to bulk-like H_3PW (inset in Fig. 3) become apparent as H_3PW loading reaches maximum of 50 wt.% (Fig. 3). This implies that the clusters of Keggin ions may exist on $Ce_{0.5}Zr_{0.5}O_2$ support. To summarize, the present FT-IR and FT-Raman study of Keggin units dispersed on $Ce_{0.5}Zr_{0.5}O_2$ support shows unique differences in vibrational frequencies which can be correlated to the primary Keggin anions interacting with Lewis sites involving mainly Ce^{4+} ions and Zr^{4+} ions, thus affecting the P–O bond, W=$O_{terminal}$ bond and W–$O_{central}$ bond. The changed vibrational spectral shapes are more pronounced in IR spectra than in Raman spectra.

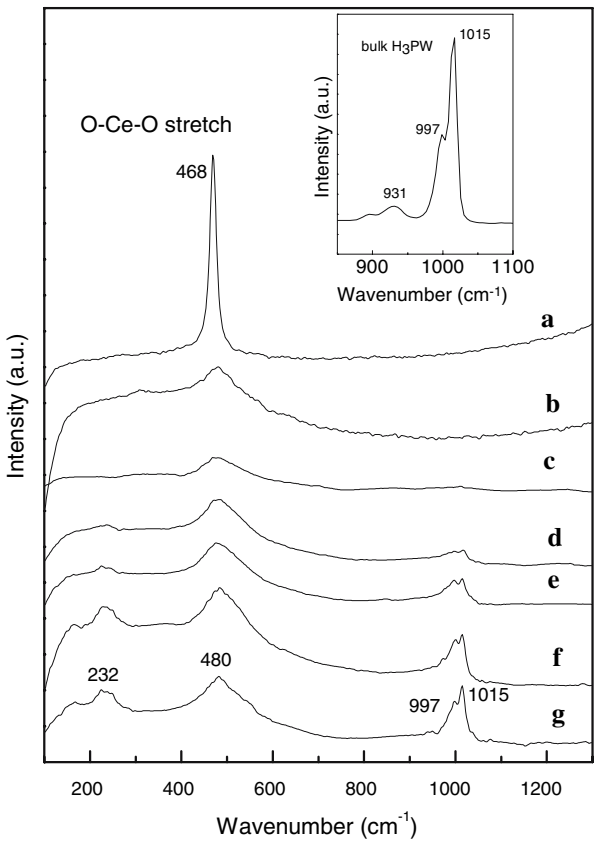

Fig. 3 Raman spectra of (**a**) CeO_2, (**b**) $Ce_{0.5}Zr_{0.5}O_2$, (**c**–**g**) 10, 20, 30, 40, 50 wt.% of H_3PW dispersed on $Ce_{0.5}Zr_{0.5}O_2$ support

3.4 ^{31}P MAS NMR Study

The Keggin anions of H_3PW have been extensively characterized by ^{31}P MAS NMR, which provides structural and bonding information of the anions interacting with various supports [11, 14–16, 18, 23, 35, 39]. The ^{31}P MAS NMR can identify and differentiate between various polyanions, $H_nPW_{12}O_{40}^{n-3}$ (n = 0, 1, 2, 3), interacting with surface metal ions such as Ce^{4+} in $Ce_{0.5}Zr_{0.5}O_2$ support. Figure 4 shows the ^{31}P MAS NMR spectra of H_3PW and 10–50 wt.% H_3PW supported on $Ce_{0.5}Zr_{0.5}O_2$ samples calcined at 250 °C. As reported in the literature [11, 14, 23], the ^{31}P MAS NMR spectrum of bulk solid H_3PW sample shows a sharp and symmetric resonance peak around –15 ppm

characteristic of phosphorus in the central position of a Keggin unit. This resonance peak has become asymmetrically broad and shifted to up-field (~ –16.4 ppm) as a function of H_3PW loading (Fig. 4). The 10 wt.% H_3PW supported on $Ce_{0.5}Zr_{0.5}O_2$ solid solution shows a broad peak at –15 ppm suggesting that the Keggin units are not collapsed on the surface (Fig 4b). Starting from 40 wt.% H_3PW loading, multiple resonance shoulders begin to appear at around –15 and –14 ppm, in addition to the main resonance peak at –16.4 ppm showing the presence of several components. The single peak at –15 ppm in the ^{31}P NMR spectrum generally indicates that the Keggin structure is retained (also confirmed by FTIR). The –14.2 ppm ^{31}P NMR signal may arise from the lacunary (defect) heteropolyanions such as $PW_{11}O_{39}^{7-}$ or $P_2W_{17}O_{61}^{10-}$ reported in the literature [40]. The up-field peaks appear to be due to the formation of $(M^{4+})(H_2PW_{12}O_{40}^{-})$, $(M^{4+})(HPW_{12}O_{40}^{2-})$ and $(M^{4+})(PW_{12}O_{40}^{3-})$ surface species either on Ce^{4+} sites or Zr^{4+} sites. The Keggin anions can be anchored on the positive metal ion sites leading to the formation of variety of surface species. Moreover, the Keggin ion strongly interacting with pure ZrO_2 support shows broad ^{31}P MAS NMR peaks centered at –12.8 ppm [41] and –12 ppm due to P–OH in the Keggin units [42, 43]. The observed ^{31}P chemical shifts on $Ce_{0.5}Zr_{0.5}O_2$ support are not in agreement with those reported on ZrO_2 and zeolite supports [14–16, 23]. However, the linewidth which is about 0.5 ppm for pure H_3PW, has increased to about 2.5 ppm with a chemical shift at 16.4 ppm for Keggin ions on $Ce_{0.5}Zr_{0.5}O_2$ indicating a stronger interaction between them. This may be due to better stability of Keggin anions on Ce^{4+} ions by charge exchange between O 2*p* orbital and Ce 4f5d6s outer orbital configuration than Zr 4*d*5*s* outer orbital configuration. As H_3PW loading is increased the emergence of bulk like H_3PW species at –15 ppm is also seen along with the proposed surface PW species, particularly at 50 wt.% H_3PW loading. This study shows the deposition of T_d symmetric $PW_{12}O_{40}^{3-}$ molecular heteropolyanions on the $Ce_{0.5}Zr_{0.5}O_2$ support and the distortion of T_d symmetry due to their interaction with Ce^{4+} and Zr^{4+} ions. The distortion is manifested as new vibrational features in IR spectra and spectral shifts in ^{31}P MAS NMR (Figs. 2–4 and Table 2). The stable $PW_{12}O_{40}^{3-}$ ions and $CeW_{10}O_{36}^{8-}$ species have been observed earlier on highly ordered pyrolytic graphite (HOPG) using AFM and STM studies [44]. The electronic structure of these ions is described in terms of valence band composed of HOMOs of oxygen *p* character and the conduction band composed of LUMOs of metal *d* character. The valence band electrons are readily shared with cation centres forming stable Keggin anions on $Ce_{0.5}Zr_{0.5}O_2$ oxide surface.

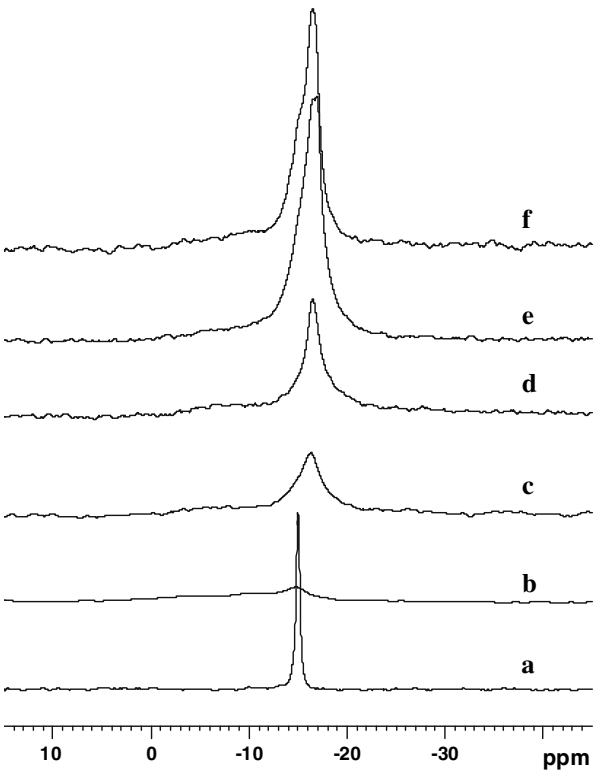

Fig. 4 ^{31}P MAS NMR spectra of (**a**) H_3PW, (**b**–**f**) 10, 20, 30, 40, 50 wt.% of H_3PW dispersed on $Ce_{0.5}Zr_{0.5}O_2$ support

3.5 TPR Study

Temperature programmed reduction technique has been extensively used to study the reduction properties of $Ce_xZrO_{1-x}O_2$ solid solutions [45, 46] as well as heteropoly acids [47]. This technique can provide sensitive information on redox properties, valence states of metal ions at various stages of reduction, catalyst composition, surface area correlations and nature of supported species-support

Table 2 FT-IR and Raman frequencies of H_3PW Keggin units dispersed on $Ce_{0.5}Zr_{0.5}O2$ solid solution

Vibrational	IR for species (i) (cm^{-1})	IR for species (ii) (cm^{-1})	Raman (cm^{-1})	^{31}P MAS NMR
ν_{p-0}	1080	1051		–15 ppm[a]
$\nu W{=}O_{terminal}$	982	957	1015 (sym)	–16.4 ppm[b]
			997 (asym)	–16.4 ppm[b]
$\nu W{-}O_{corner}{-}W$	892	–	–	–14.2 ppm[c]
$\nu W{-}O_{edge}{-}W$	812	–	–	
$\nu O{-}Ce{-}O$	–	–	468	
$\nu W{=}O_{central}$	–	–	232	

[a] $H_3PW_{12}O_{14}$

[b] $(Ce^{4+})H_nPW_{12}O_{40}^{n-3}$ (n = 0, 1, 2, 3)

[c] $PW_{11}O_{39}^{7-}$ or $P_2W_{17}O_{61}^{10-}$

interactions. The TPR profiles of cubic CeO_2 (inset), $Ce_{0.5}Zr_{0.5}O_2$, 10–50 wt.% of H_3PW on $Ce_{0.5}Zr_{0.5}O_2$ support and pure H_3PW samples are presented in Fig. 5. The reduction of $Ce_{0.5}Zr_{0.5}O_2$ support occurs in a single step at 528 °C, unlike CeO_2 (41 m^2 g^{-1}), which is reduced in two steps at 460 and 770 °C. It has been reported that the $Ce_xZr_{1-x}O_2$ solid solutions undergo single reduction in the temperature region of 300–700 °C depending on the cerium content [45, 46]. The mechanism of reduction involves adsorbed hydrogen, and both surface and bulk O^{2-} and Ce^{4+} ions. In the present case, the reduction peak at 528 °C of $Ce_{0.5}Zr_{0.5}O_2$ is shifted to 590 °C in the presence of Keggin units present on the surface (Fig. 5c). When surface Ce^{4+} and Zr^{4+} ions are blocked as Ce^{4+}–O–W and Zr^{4+}–O–W by Keggin molecular layers, the surface sites (O^{2-} and Ce^{4+}) where reduction process begins, are not accessible to hydrogen adsorption and diffusion. Moreover, the surface Ce^{4+} ions may have already been present in partly reduced state due to stronger interaction with Keggin molecular ions. As a result the reduction process is hindered and shifted to higher temperatures. Above 25 wt.% of H_3PW, the reduction profile has changed significantly in Fig. 5 indicating surface structural changes in Keggin molecular layers. This observation corroborates with the proposed molecular layer of Keggin units below 25 wt.% of H_3PW on $Ce_{0.5}Zr_{0.5}O_2$, discussed in Sect. 3.1. At higher loadings of H_3PW (spectra *d-f* in Fig. 5), the reduction occurred in three regions at 430–530, 530–630 and 630–780 °C. The three-peak reduction is typical of bulk-like heteropoly compounds as reported by Hodnett and Moffat [47]. The reduction that occurred up to 530 °C is attributed to deprotonation and removal of lattice oxygen of Keggin units (step 1 below) as well as the reduction contribution of ceria component. A separate IR study showed the decomposition of Keggin ions on $Ce_{0.5}Zr_{0.5}O_2$ surface occurs around 540 °C. Therefore, above 530 °C the Keggin ions decompose to give WO_3 (step 2 below and Fig. 5g) which is further reduced to lower oxidation states giving rise to reduction peaks at 570 and 700 °C.

$$\left.\begin{aligned} H_3PW_{12}O_{40}\cdot 6H_2O &\xrightarrow{\leq 530^\circ C} PW_{12}O_{38.5} + 7.5H_2O \\ Ce_{0.5}Zr_{0.5}O_2 + xH_2 &\xrightarrow{\leq 530^\circ C} Ce_{0.5}Zr_{0.5}O_{2-x} + xH_2O \end{aligned}\right\} \quad (1)$$

$$PW_{12}O_{38.5} \xrightarrow{> 530^\circ C} 12WO_3 + \frac{1}{2}P_2O_5 \quad (2)$$

However, the reduction peak of 50 wt.% H_3PW above 550°C is not as intense as that of the bulk H_3PW shown in Fig. 5g. The observed differences between the bulk and $Ce_{0.5}Zr_{0.5}O_2$-supported H_3PW, suggest that the Keggin ions are packed as molecular layers.

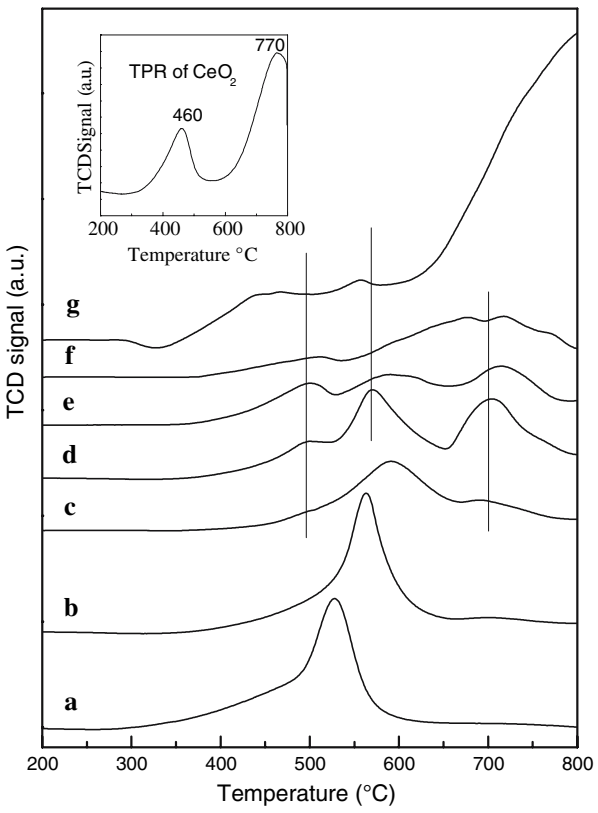

Fig. 5 TPR profile of (**a**) $Ce_{0.5}Zr_{0.5}O_2$, (**b–f**) 10, 20, 30, 40, 50 wt.% of H_3PW dispersed on $Ce_{0.5}Zr_{0.5}O_2$ support, and (**g**) pure H_3PW. Inset is the TPR of CeO_2 sample

3.6 NH_3-TPD Study

The ammonia adsorption–desorption technique is helpful to determine total number of sites (total acidity) and the strength of sites (i.e., temperature dependency) present on catalyst surfaces. The acid properties of dispersed Keggin molecular ion layers on $Ce_{0.5}Zr_{0.}5O_2$ solid solution support are analysed by TPD of ammonia. The NH_3-TPD profiles of $Ce_{0.5}Zr_{0.5}O_2$, 10–50 wt.% of H_3PW on $Ce_{0.5}Zr_{0.5}O_2$ support and pure H_3PW samples investigated are shown in Fig. 6. The clean $Ce_{0.5}Zr_{0.5}O_2$ support shows weaker desorption profiles of NH_3 at less than 215 °C. Stronger desorption profiles are observed at 215–380 and 440–640 °C. The trend of NH_3 desorption from $Ce_{0.5}Zr_{0.5}O_2$ is found to be complex and reflects several adsorption sites available for adsorbate molecules. The preparation method seems to have distinct influence on the nature and distribution of surface acidic sites on $Ce_xZr_{1-x}O_2$ samples. The NH_3–TPD behaviour of sol–gel combustion synthesized $Ce_{0.5}Zr_{0.5}O_2$ sample in this study exhibits wider distribution of weaker as well as stronger acidic sites when compared to the distribution below

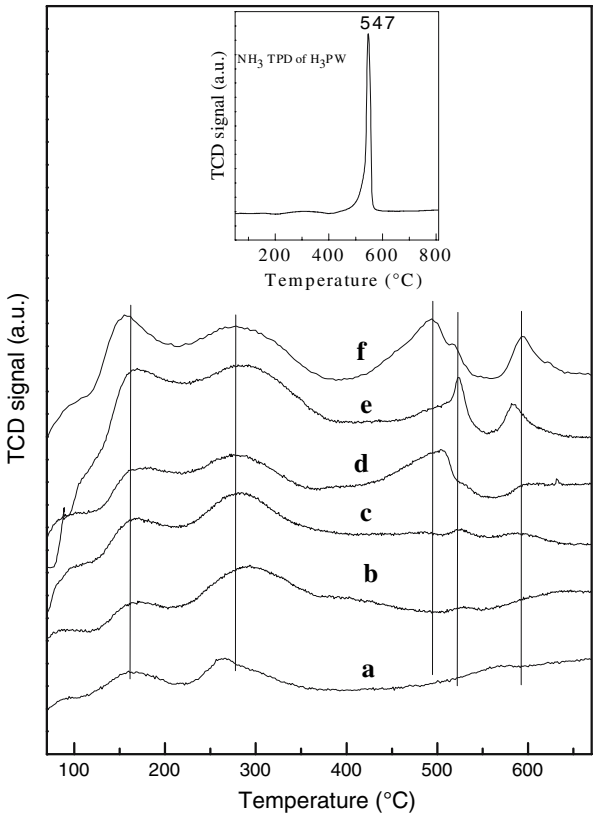

Fig. 6 NH_3–TPD profile of (**a**) $Ce_{0.5}Zr_{0.5}O_2$, (**b**–**f**) 10, 20, 30, 40, 50 wt.% of H_3PW dispersed on $Ce_{0.5}Zr_{0.5}O_2$ support. Inset is the TPD of pure H_3PW

500 °C reported on ZrO_2 and $Ce_xZr_{1-x}O_2$ samples prepared by precipitation method [35, 48]. In general, this study shows two categories of acidic adsorption sites in Fig. 6. The multiple weaker acidic sites below 400 °C, which resemble to those sites on $Ce_xZr_{1-x}O_2$ support and the stronger acidic sites above 400 °C are attributable to ammonia interacting with Keggin molecular layers (compare with inset in Fig. 6). Ammonia desorption from 12-tungstophosphoric acid molecular layers at higher temperatures is consistent with literature reports [49] and accordingly the desorption peaks between 400 and 550 °C are assigned to ammonia released from tungstophosphoric acid molecular layers. However, the high temperature desorption peaks around 590 °C is more likely from collapsed Keggin units. It appears that there are two kinds of sites, (i) below 25 wt.% H_3PW loading the adsorption sites are due to the Keggin ions strongly interacting with $Ce_{0.5}Zr_{0.5}O_2$ support and (ii) above 25 wt.%, NH_3 uptake occurs on $H_nPW_{12}O_{40}^{n-3}$ (n = 1, 2, 3) ions in the upper layers, in addition to ammonia molecules directly interacting with $Ce_{0.5}Zr_{0.5}O_2$ support. The NH_3–TPD study also indicates the occurrence of variety of adsorption sites on bare $Ce_{0.5}Zr_{0.5}O_2$ support as well as those present on Keggin molecular ions deposited on the oxide.

Table 3 TPR and TPD peak temperatures of H_3PW Keggin molecular units dispersed on $Ce_{0.5}Zr_{0.5}O_2$ solid solution

Sample	H_2-TPR peaks (°C)	NH_3-TPD peaks (°C)
CeO_2	460, 770	–
$Ce_{0.5}Zr_{0.5}O_2$	528	167, 283, 563, 760
H_3PW	440, 557, >640	547
10 wt.% $H_3PW/Ce_{0.5}Zr_{0.5}O_2$	563[a]	(167, 283)[a], (490, 525, 591)[b]
20 wt.% $H_3PW/Ce_{0.5}Zr_{0.5}O_2$	590[a]	(167, 283)[a], (490, 525, 591)[b]
30 wt.% $H_3PW/Ce_{0.5}Zr_{0.5}O_2$	496, 569, 700	(167, 283)[a], (490, 525, 591)[b]
40 wt.% $H_3PW/Ce_{0.5}Zr_{0.5}O_2$	496, 588, 712	(167, 283)[a], (490, 525, 591)[b]
50 wt.% $H_3PW/Ce_{0.5}Zr_{0.5}O_2$	510, 712	(167, 283)[a], (490, 525, 591)[b]

[a] Peak related to oxide support

[b] Peak related to Keggin ion layers on the support

The Keggin ions seem to have been arranged in the form of layers on the $Ce_{0.5}Zr_{0.5}O_2$ support and the driving force for such arrangement could come from the first layer of Keggin units interacting with the surface unsaturated metal ions to originate Ce^{4+}–O–W and Zr^{4+}–O–W bonds. This intimate interaction perturbs the chemical environment mostly in the first layer Keggin units ($H_2PW_{12}O_{40}^-$, $HPW_{12}O_{40}^{2-}$ and $PW_{12}O_{40}^{3-}$), since they interact with terminal W=O units. The evidence from IR, Raman, NMR (Table 2), TPR and TPD (Table 3) are in agreement with this interpretation. At higher loadings the perturbation subsides and variety of Keggin species are present on the support. However, interaction with the $Ce_{0.5}Zr_{0.5}O_2$ support diminishes at higher loadings, which may lead to the formation of three dimensional Keggin islands. Such deposition mechanism can be described as Stranski–Krastanov mechanism, which can be best studied on well-defined single crystal $Ce_{0.5}Zr_{0.5}O_2$ supports.

3.7 UV–Vis DRS Study

The UV–Vis DRS spectral features are generally indicative of charge transfer processes in $Ce_xZr_{1-x}O_2$ oxides and Keggin anions [2, 35, 50]. The DRS spectra can give information on surface coordination and different oxidation states of metal ions present in the samples by measuring the *d–d*, *f–d* transitions and oxygen–metal ion charge transfer bands. The UV–Vis DRS spectra of pure H_3PW, H_3PW dispersed on $Ce_{0.5}Zr_{0.5}O_2$ and oxide support are presented in Fig. 7. The charge transfer absorption bands of heteropolyanions appear in the near UV region of 200–350 nm,

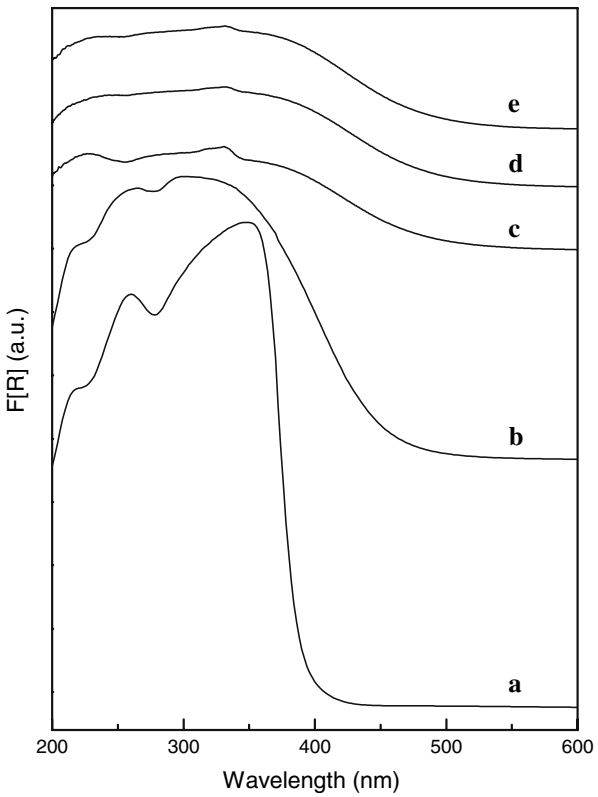

Fig. 7 UV–Vis diffuse reflectance spectra of (**a**) H_3PW, (**b**) $Ce_{0.5}Zr_{0.5}O_2$, (**c–e**) 20, 40, 50 wt.% of H_3PW dispersed on $Ce_{0.5}Zr_{0.5}O_2$ support

which can be ascribed to oxygen-to-metal charge transitions. Accordingly pure H_3PW shows two intense charge transfer bands at 259 and ~330 nm, and a weak band at 217 nm in Fig. 7a. All Keggin ions generally show a charge transfer band at 260 nm, which is well resolved in the case of H_3PW than any other Keggin species. The absorption bands correspond to the ligand to metal charge transfer ($O^{2-} \rightarrow W^{6+}$) in the Keggin polyanions. The two absorption peaks at 259 and ~330 nm are interpreted as O → W charge transfer absorptions where W atoms are located in W–O_e–W intra bridges between edge-sharing and W–O_c–W inter bridges between corner-sharing WO_6 octahedra. The band at 217 nm appears to be due to O → P transition. The DRS spectrum of $Ce_{0.5}Zr_{0.5}O_2$ shows broad absorption bands in the region of 200–450 nm due to $O^{2-} \rightarrow W^{4+}$ transition of low-coordinated Ce^{4+} ions, $O^{2-} \rightarrow Zr4^{+}$ and $f \rightarrow d$ transitions of Ce^{3+} ions [2]. With the dispersion of H_3PW on $Ce_{0.5}Zr_{0.5}O_2$, all the transitions related to the support and the Keggin ion have lost intensity and spread widely due to considerable overlap and collective absorption of various species present on the surface. The intensity loss of the Keggin ion charge transfer bands at 217, 259 and ~330 nm shows that these ions are not packed as in their secondary structure but spread on the support interacting with metal ions on $Ce_{0.5}Zr_{0.5}O_2$ surface.

3.8 SEM and TEM Studies

The SEM and HRTEM pictures of $Ce_{0.5}Zr_{0.5}O_2$ with dispersed H_3PW layers are shown in Fig. 8. The SEM and TEM pictures essentially show large flakes of $Ce_{0.5}Zr_{0.5}O_2$ particles (Fig. 8a–c) on which Keggin ion patches of about 5 nm size (Fig. 8d) are dispersed. It cannot be ruled out that, at lower loadings, some patches may have more than one molecular layer thick Keggin units on $Ce_{0.5}Zr_{0.5}O_2$ support. The flake-like nature of $Ce_{0.5}Zr_{0.5}O_2$ particles is more pronounced at 50 wt.% of H_3PW (Fig. 8c). The presence of nano-size Keggin units on $Ce_{0.5}Zr_{0.5}O_2$ flakes can be clearly seen in the HRTEM picture of 20 wt.% $H_3PW/Ce_{0.5}Zr_{0.5}O_2$ sample. The patches of $Ce_{0.5}Zr_{0.5}O_2$ and H_3PW Keggin units are marked in the HRTEM picture (Fig. 8d). The support patches show parallel planes of (001) orientation, which are normally observed in the microcrystals of mixed oxides of ceria [51]. The HRTEM picture also shows the Keggin ions uniformly spread on $Ce_{0.5}Zr_{0.5}O_2$ support and there is no evidence for Keggin ion segregation as large nanocrystallites or bigger aggregates on the support. It has been reported that bulk heteropoly acid salts aggregate into spherical and dodecahedral shapes, ascertained by SEM [18].

3.9 Reaction Study

A test reaction of acetophenone conversion on Keggin units dispersed on $Ce_{0.5}Zr_{0.5}O_2$ solid solution has been carried out. The conversion of acetophenone to styrene in vapour phase is optimized for different mole ratios of acetophenone and isopropanol in the temperature range 200–300 °C. The conversion is found to be maximum around 1:5 mole ratio of acetophenone to isopropanol at 250 °C (Fig. 9). The catalytic activity of Keggin ions supported on $Ce_{0.5}Zr_{0.5}O_2$ solid solution has been tested under these conditions. Figure 10 shows the activity of Keggin ions as a function of H_3PW loading on $Ce_{0.5}Zr_{0.5}O_2$ support. It also shows the relative intensities of IR shoulder peaks at 1051 cm^{-1} (ν_{P-O}) and 957 cm^{-1} ($\nu_{W=O}$) affected by the interaction of Keggin ions with Ce^{4+} ions. The catalytic activity is peaked at 20 wt.% of H_3PW loading on $Ce_{0.5}Zr_{0.5}O_2$ support indicating that the molecular layer-region Keggin ions interacting with cerium or zirconium ions are active for this reaction. The relative intensities of IR shoulder peaks are a measure of number of structurally perturbed Keggin ions, which decrease rapidly as a function of HPA loading on $Ce_{0.5}Zr_{0.5}O_2$ solid solution. There is a correlation between the loss of activity and decreased number of perturbed Keggin ions above 20 wt.% of H_3PW dispersion. However, for 10 wt.% H_3PW on $Ce_{0.5}Zr_{0.5}O_2$, the activity is lower due to smaller amount of Keggin units available for the

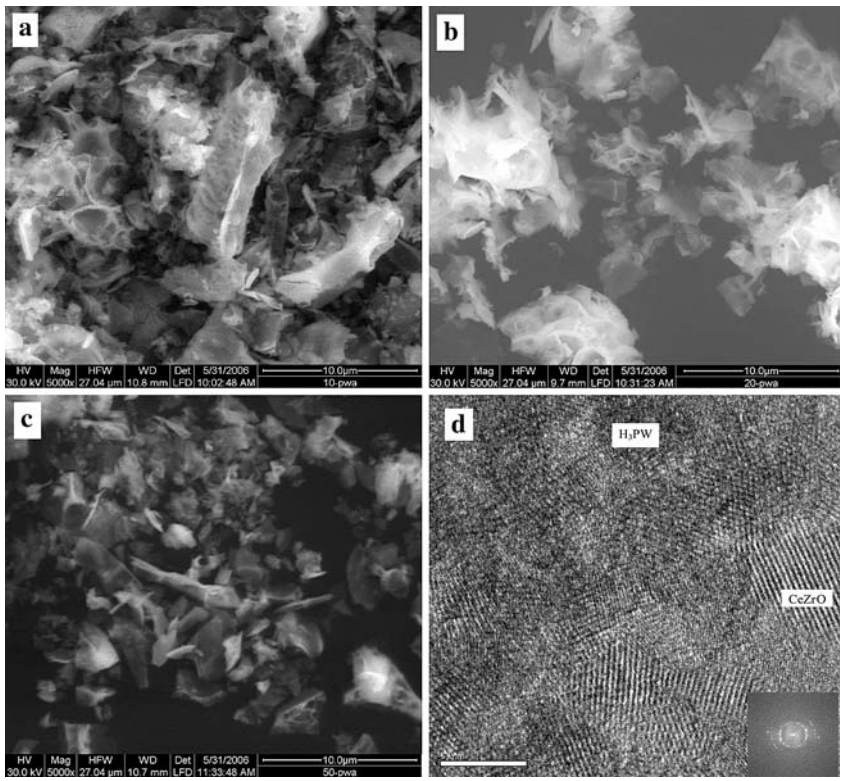

Fig. 8 SEM pictures of (**a**) 10 wt.%, (**b**) 20 wt.% and (**c**) 50 wt.% of H_3PW dispersed on $Ce_{0.5}Zr_{0.5}O_2$ support, and (**d**) TEM picture of (**b**)

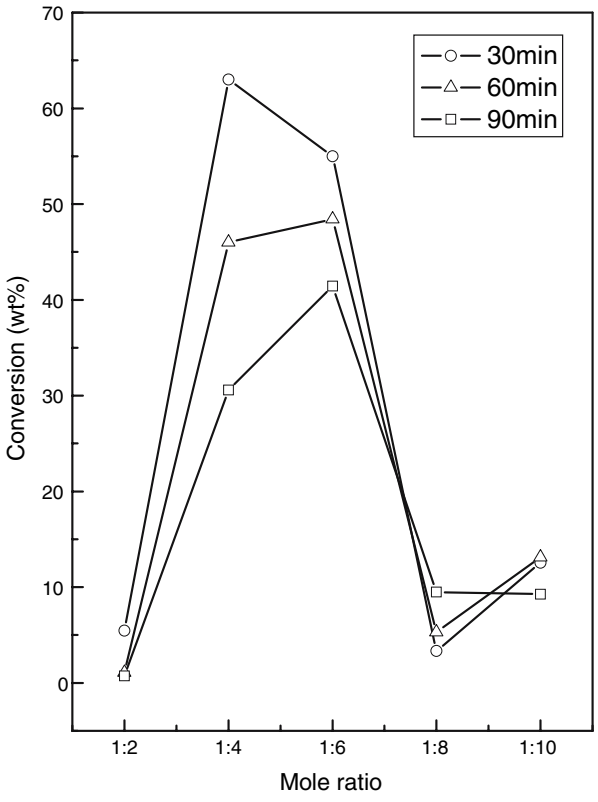

Fig. 9 Conversion of acetophenone as a function of mole ratio of reactants at 250 °C on 20 wt.% $H_3PW/Ce_{0.5}Zr_{0.5}O_2$ catalyst at different time intervals

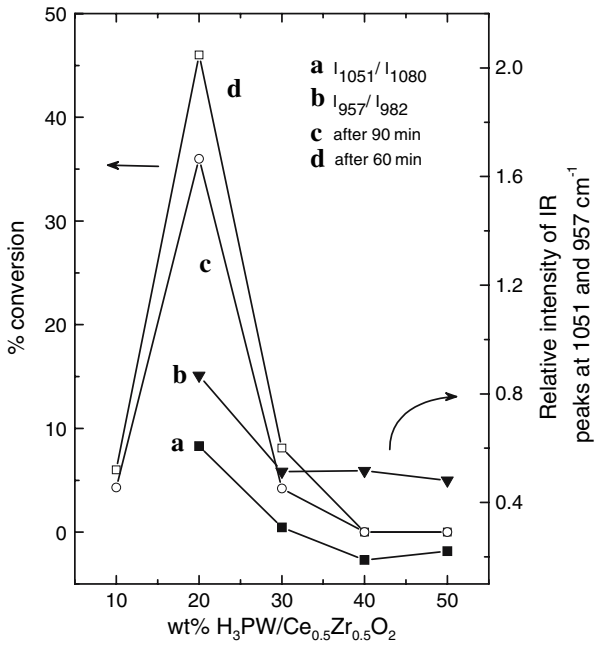

Fig. 10 Vapour phase conversion of acetophenone to styrene on 20 wt.% $H_3PW/Ce_{0.5}Zr_{0.5}O_2$ catalysts. Correlation is made between the conversion and relative intensities of IR bands of Keggin ions interacting with surface Ce^{4+}/Zr^{4+} ions

reaction, which is evident from IR spectrum (Fig 2b) and ^{31}P MAS NMR spectrum (Fig. 4b). Several recent studies [14–16] reported the existence of perturbed and unperturbed

Keggin anions, present on the zeolite supports and inside the cages, due to the nature of their chemical interaction and exhibit different chemical reactivity and selectivity. Newman et al. [22] observed similar trend of forming an interfacial layer of tungstophosphoric acid on silica surface where H_3PW phase contains two distinct tungstate environments within a molecular layer and then approaching the bulk-like environment within the multilayers. The Keggin ion clusters perturbed by close proximity to silica surface exhibit higher activity towards isomerisation of α-pinene. In the present study, the Keggin ions of $H_3PW_{12}O_{40}$ dispersed on $Ce_{0.5}Zr_{0.5}O_2$ show similar trend where the perturbed interfacial Keggin species on the redox support seems to exhibit activity for vapour phase conversion of acetophenone to styrene.

The mechanism of acetophenone conversion to styrene involves two steps as shown in Scheme 2. In the first step both Ce^{4+} and Zr^{4+} metal ion sites may be involved in hydrogen transfer MPV reduction reaction. The reductant, 2-propanol, chemisorbs on metal or oxygen sites along with acetophenone, which is coordinated to metal ions. This can form cyclic transition state proposed in earlier studies [9, 52–55]. This step is followed by dehydration of alcohol in the presence of H_3PW leading to the formation of styrene. A maximum of about 60% conversion with 100% selectivity to styrene can be obtained under optimum conditions on 20 wt.% $H_3PW/Ce_{0.5}Zr_{0.5}O_2$ catalysts. However, the catalyst activity is found to be high up to 120 min and decreased rapidly with time. Chuah and co-workers [53] recently reported 18.3% acetophenone conversion in 5 h on a monolayer of zirconium 1-propoxide grafted SBA-15 catalysts. It appears that active sites are blocked by water formed during the dehydration step, which may cause the deactivation of 20 wt.% $H_3PW/Ce_{0.5}Zr_{0.5}O_2$ catalyst.

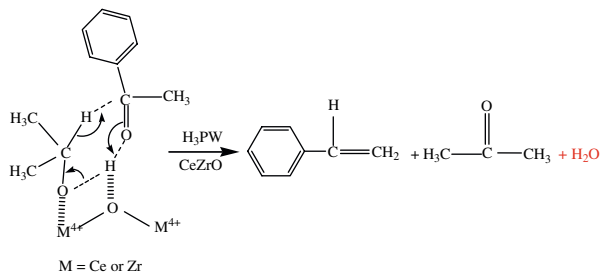

Scheme 2 Proposed mechanism of acetophenone conversion on CeZrO in the presence of H_3PW species

4 Conclusions

The powder $Ce_{0.5}Zr_{0.5}O_2$ solid solution prepared by sol–gel combustion is a suitable support to prepare 10–50 wt.% H_3PW catalysts. XRD does not show the presence of Keggin ions on $Ce_{0.5}Zr_{0.5}O_2$ solid solution at all loadings. However, Keggin ions present in the initial layer of H_3PW on oxide support show split IR bands. The IR bands at 1080 cm^{-1} (ν_{P-O}) and 982 cm^{-1} ($\nu_{W=O,terminal}$) are due to the unperturbed Keggin ions, while those at 1051 cm^{-1} (ν_{P-O}) and 957 cm^{-1} ($\nu_{W=O,terminal}$) are due to perturbed Keggin ions present on $Ce_{0.5}Zr_{0.5}O_2$ surface. At higher coverages of H_3PW, IR peaks of perturbed Keggin ions disappear due to the formation of bulk-like H_3PW phase. The Raman band at 468 cm^{-1} is characteristic of O–Ce–O stretching of bulk CeO_2 which is asymmetrically broadened towards lower frequencies upon substitution of 0.5 mol of Zr^{4+} ions. The Raman bands are attributed to $Ce^{4+}\cdots O^{\delta-}_{terminal}$=W and $Zr^{4+}\cdots O^{\delta-}_{terminal}$=W bonds formed between surface metal ions and $H_nPW_{12}O^{n-3}_{40}$ (n = 0, 1, 2, 3) species. ^{31}P MAS NMR data show the existence of perturbed Keggin species between –16.1 and –16.9 ppm on $Ce_{0.5}Zr_{0.5}O_2$ solid solution. These Keggin ions are packed as molecular layers on $Ce_{0.5}Zr_{0.5}O_2$ support and their H_2-TPR behaviour is quite different to that of bulk H_3PW. The NH_3-TPD study indicates various adsorption sites on bare $Ce_{0.5}Zr_{0.5}O_2$ support as well as on Keggin molecular ion layers. The UV–Vis DRS spectra show two absorption peaks at 259 and ~330 nm due to O → W charge transfer absorptions where W atoms are connected to edge and corner sharing oxygens of W–O–W bridges in the Keggin anion. These results along with SEM and TEM pictures suggest that Keggin units are spread in the form of molecular layer patches on $Ce_{0.5}Zr_{0.5}O_2$ support. The perturbed Keggin units of 20 wt.% H_3PW on $Ce_{0.5}Zr_{0.5}O_2$ support are active for vapour phase conversion of acetophenone to styrene, which occurs via the formation of cyclic intermediate on Ce^{4+} or Zr^{4+} Lewis sites. The maximum conversion of acetophenone is 63% with 100% styrene selectivity on 20 wt.% $H_3PW/Ce_{0.5}Zr_{0.5}O_2$.

Acknowledgment The first author would like to thank the Defence Research and Development Organization (DRDO), New Delhi, for providing financial support under Grant No. ERIP/ER/0300231/M/01.

References

1. DiMonte R, Kašpar J (2005) J Mater Chem 15:633
2. Ranga Rao G, Sahu HR (2001) Proc Indian Acad Sci Chem Sci 113:651
3. Tomishige K, Kunimori K (2002) Appl Catal A Gen 237:103
4. Tomishige K, Furusawa Y, Ikeda Y, Asadullah M, Fujimoto K (2001) Catal Lett 76:71
5. Sato S, Takahashi R, Sodesawa T, Yamamoto N (2004) Catal Commun 5:397
6. Mishra BG, Ranga Rao G (2006) J Mol Catal A Chem 243:204
7. Solinas V, Rombi E, Ferino I, Cutrufello MG, Colón G, Navío JA (2003) J Mol Catal A Chem 204–205:629
8. Hamoudi S, Sayari A, Belkacemi K, Bonneviot L, Larachi F (2000) Catal Today 62:379

9. Ranga Rao G, Sahu HR, Mishra BG (2003) React Kinet Catal Lett 78:151
10. Cutrufello MG, Ferino I, Solinas V, Primavera A, Trovarelli A, Auroux A, Picciau C (1999) Phys Chem Chem Phys 1:3369
11. Kuang W, Rives A, Fournier M, Hubaut R (2003) Appl Catal A Gen 250:221
12. Dias JA, Caliman E, Dias SCL, Paulo M, de Souza ATCP (2003) Catal Today 85:39
13. Izumi Y, Hasebe R, Urabe K (1983) J Catal 84:402
14. Sulikowski B, Haber J, Kubacka A, Pamin K, Olejniczaka Z, Ptaszyński J (1996) Catal Lett 39:27
15. Olejniczak Z, Sulikowski B, Kubacka A, Gąsior M (2000) Topics Catal 11/12:391
16. Sulikowski B, Rachwalik R (2003) Appl Catal A 256:173
17. Watanabe Y, Yamamoto K, Tatsumi T (1999) J Mol Catal A Gen 145:281
18. Misono M (2001) Chem Comm 1141
19. Nowińska K, Fiedorow R, Adamiec J (1991) J Chem Soc Faraday Trans 87:749
20. Misono M (1988) Catal Rev Sci Eng 30:339
21. Gomez-Garcia MA, Pitchon V, Kiennemann A (2005) Environ. Sci Technol 39:638
22. Newman AD, Lee AF, Wilson K, Young NA (2005) Catal Lett 102:45
23. Kozhevnikov IV, Kloetstra KR, Sinnema A, Zandbergen HW, van Bekkum H (1996) J Mol Catal A Chem 114:287
24. Klemperer WG, Wall CG (1998) Chem Rev 98:297
25. Pierre AC (1991) Ceram Bull 70:1281
26. Muthuraman M, Patil KC (1998) Mater Res Bull 33:655
27. Kaspar J, Fornasiero P, Balducci G, Di Monte R, Hickey N, Sergo V (2003) Inorg Chim Acta 349:217
28. Kishimoto H, Omata T, Otsuka-Yao-Matsuo S, Ueda K, Hosono H, Kawazoe H (2000) J Alloys Compd 312:94
29. Okuhara T, Mizuno N, Misono M (1996) Adv Catal 41:113
30. Rocchiccioli-Deltcheff C, Fournier M, Franck R (1983) Inorg Chem 22:207
31. Escribano VS, López EF, Panizza M, Resini C, Amores JMG, Busca G (2003) Solid State Sci 5:1369
32. Kanakaraju S, Mohan S, Sood AK (1997) Thin Solid Films 305:191
33. Dutta G, Waghmare UV, Baidya T, Hegde MS, Priolkar KR, Sarode PR (2006) Catal Lett 108:165
34. Fernández-García M, Martínez-Arias A, Iglesias-Juez A, Belver C, Hungría AB, Conesa JC, Soria J (2000) J Catal 194:385
35. Devassy BM, Halligudi SB (2005) J Catal 236:313
36. Loridant S, Feche C, Essayem N, Figueras F (2005) J Phys Chem B 109:5631
37. Scheithauer M, Grasselli RK, Knözinger H (1998) Langmuir 14:3019
38. López-Salinas E, Hernández-Cortéz JG, Schifter I, Torres-Garćia E, Navarrete J, Gutiérrez-Carrillo A, López T, Lottici PP, Bersani D (2000) Appl Catal A Gen 193:215
39. Dias JA, Osegovic JP, Drago RS (1999) J Catal 183:83
40. Dias AS, Pillinger M, Valente AA (2006) Micropor Mesopor Mater 94:214
41. Angelis A, Amarilli S, Berti D, Montanari L, Perego C (1999) J Mol Catal A Chem 146:37
42. Devassy BM, Halligudi SB, Hegde SG, Halgeri AB, Lefebvre F (2002) Chem Commun 1074
43. Devassy BM, Lefebvre F, Halligudi SB (2005) J Catal 231:1
44. Klemperer WG, Wall CG (1998) Chem Rev 98:297
45. Fonasiero P, Di Monte R, Ranga Rao G, Kaspar J, Meriani S, Trovarelli A, Graziani M (1995) J Catal 151:168
46. Ranga Rao G (1999) Bull Mater Sci 22:89
47. Hodnett BK, Moffat JB (1985) J Catal 91:93
48. Ortiz JIG, de Rivas B, Fonseca RL, Velasco JRG (2006) Appl Catal B Environ 65:191
49. Hodnett BK, Moffat JB (1984) J Catal 88:253
50. He T, Yao J (2006) Prog Mater Sci 51:810
51. Bernal S, Calvino JJ, Gatica JM, Cartes CL, Pintado JM (2002) In: Trovarelli A (ed) Catalysis by ceria and related materials, vol. 2, Ch. 4. Imperial College Press, London
52. Kumbhar PS, Sanchez-Valente J, Lopez J, Figueras F (1998) Chem Commun 535
53. Zhu Y, Jaenicke S, Chuah GK (2003) J Catal 218:396
54. Zhu Y, Liu S, Jaenicke S, Chuah G (2004) Catal Today 97:249
55. Zhu Y, Chuah GK, Jaenicke S (2006) J Catal 241:25